

Angle- and size-dependent characteristics of incoherent Raman and fluorescent scattering by microspheres. 2. Numerical simulation

Igor Veselovskii, Vadim Griaznov, Alexei Kolgotin, and David N. Whiteman

The results of numerical simulation of inelastic scattering by microspheres with the use of a dipole model are presented. The formulas that are derived speed up the computation, thereby permitting larger-sized microspheres to be studied. The angular scattering cross section and depolarization are calculated for a wide range of size parameters as well as for different orientations of incident wave polarization. Calculations performed with small incremental changes in size permit the influence of morphology-dependent resonance (MDR) on the power and angular distribution of scattered radiation to be studied. TM and TE types of MDR produce enhanced scattering of the incident wave with vertical and horizontal polarization; the corresponding shape of the phase function becomes oscillatory. Special attention is paid to the simulation of backward scattering by water droplets, which is important for Raman lidar applications. © 2002 Optical Society of America

OCIS codes: 010.1310, 010.3640, 010.7340, 290.4020, 290.5860, 290.1350.

1. Introduction

Raman and fluorescent methods are widely used in spectroscopic analysis of microparticles composition^{1–13} and biological-aerosol identification.^{14–16} One of the properties that distinguish incoherent inelastic scattering from elastic (Mie) scattering is the phase function (scattered intensity versus polar angle), which is rather smooth for inelastic scattering and has no characteristic peak in the forward direction. Another difference concerns the structure of morphology-dependent resonance (MDR). Inelastic scattering is accompanied by two types of resonance, namely, MDRs of the incident wavelength, known as input resonances, and resonances of the inelastic scattered light, known as output resonances.

For description of the inelastic process, different modifications of the dipole model are used.^{17–23} The dipole model allows phase function and the MDR to

be calculated, but numerical integration of the expressions suggested by Kerker *et al.*²⁰ is extremely time consuming. In our previous paper²⁴ we derived the formulas that permit speeding the computation; thus the inelastic scattering by microspheres can be simulated in a much more realistic manner. Here we present the angular and polarization characteristics of inelastic scatter obtained with a computer code that implements these new formulas.

The calculations are performed for transparent spheres. Though our algorithm permits computation with a complex refractive index, for now we do not consider the effects related to medium absorption. The ratio of scattered to incident wavelengths is fixed; i.e., inelastic emission occurs at a single line. Induced dipoles are parallel to the exciting field, and active molecules do not rotate during the interval between excitation and emission. This approach applies most clearly to fluorescence when dipoles are in fixed orientations (e.g., dye molecules in solids or highly viscous spheres) and to Raman scattering when the molecule is isotropically polarizable. The molecule may be considered isotropically polarizable in many cases. For example, in liquid water, which is one of the main objects of our study, the intensity of isotropic spectra exceeds that of anisotropic spectra more than an order of magnitude²⁵ (for 3200-cm⁻¹ Raman frequency and 10 C° temperature).

More-complicated models of fluorescence and Ra-

I. Veselovskii (katyv@orc.ru), V. Griaznov, and A. Kolgotin are with the Physics Instrumentation Center of General Physics Institute, Troitsk, Moscow Region, 142190, Russia. D. N. Whiteman is with the NASA Goddard Space Flight Center, Greenbelt, Maryland 20771-0001.

Received 14 February 2002; revised manuscript received 24 June 2002.

0003-6935/02/275783-09\$15.00/0

© 2002 Optical Society of America

man scattering that account for the possibility of different orientations of absorption and emission transition dipole moments and anisotropy of molecule polarizability have been presented by Druger and McNulty.^{22,23} Whereas our model corresponds to a rather idealized system, it illustrates the major effects that depend on the morphology and optical properties of the particle.

The development of a computer code of this kind is an extremely complicated issue. Probably the best criterion by which to judge a new computer code is its ability to reproduce existing experimental and computational results. There are at least several such reference points. For big particles we can expect the proportionality of the Raman signal to the volume of microsphere that was reported in numerous experimental studies.^{4,8,13} The scattering phase function should be in agreement with the computational results of Kerker and Druger²⁰ because their code describes the main features of angular distribution of the fluorescence of dye droplets.^{26,27} The depolarization of Raman scatter at 90° for an incident wave with vertical polarization should be insignificant in accordance with the experimental results of Fung and Tang.²⁸

Special attention in our simulation is paid to backscattering geometry, which is important for Raman lidar application. Raman lidars have proved to be powerful tools for the study of atmospheric water vapor,²⁹ and this technique may be extended to include Raman scattering by water droplets.^{30–33} The first experiments have demonstrated that the Raman signal from atmospheric water is significantly stronger than it should be for typical water content and the known Raman scattering cross section of bulk water.^{30–33} One possible explanation for this enhancement is an increase of the scattering phase function in the backward direction and the influence of MDR. To estimate the possible backscattering cross section and its dependence on droplet size we performed the simulation up to size parameter $x = 500$, which covers the range of possible variation of radii in nonprecipitating clouds. The results obtained demonstrate that the Raman power integrated over the MDRs is proportional to the droplet volume in a wide range of size parameters; hence the Raman technique may be used for the estimation of droplet size.³¹

2. Simulation Results

For incident radiation with vertical (V) or horizontal (H) polarization orientation with respect to the scattering plane, we calculate the intensity of scattered components with the polarization parallel to incident (H_H, V_V) as well as to depolarized (V_H, H_V) components. The program implements the formulas derived in our previous paper.²⁴ The scattered intensity is normalized to the inelastic backscatter from bulk media that contain the same number of dipoles as the microsphere does.²⁴ In numerical integration over the sphere we performed 100 angular steps, so $\Delta\theta = 1.8^\circ$ and $\Delta\varphi = 3.6^\circ$. In radial integra-

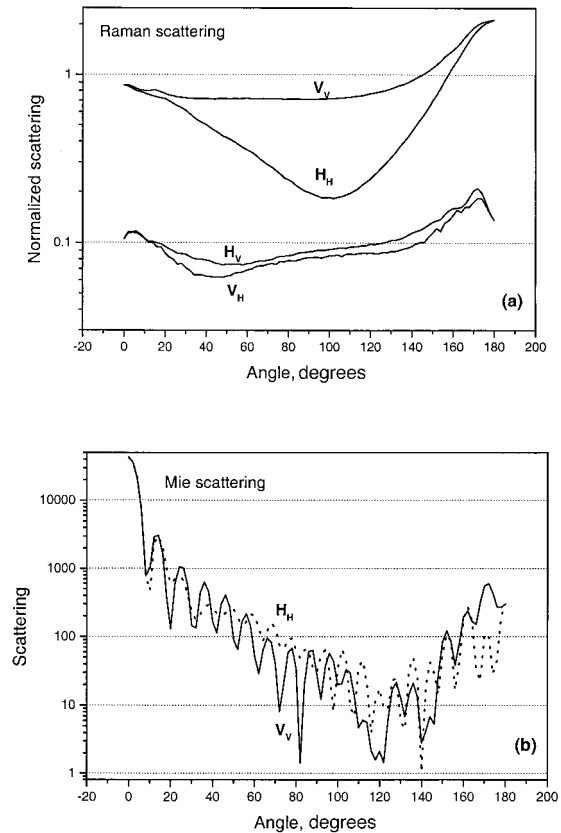


Fig. 1. Comparison of angular distribution of scattered field components for incoherent Raman and Mie scattering. The calculations were performed for size $x = 20$; angular step $\Delta\theta = 2^\circ$; refractive index $n_1 = 1.5$; and ratio $\lambda/\lambda_0 = 1.196$.

tion, usually 100 points are used; hence the integration step depends on the sphere radius. With such a number of radial points we could perform the calculations up to size $x \sim 150$ at all angles. For the backscattering geometry the computation is speeded up,²⁴ so the integration step could be decreased and calculations up to $x \sim 500$ were possible.

A. Angular Distribution

The angular distribution of all four scattered components, $V_V, H_H, V_H,$ and $H_V,$ is illustrated in Fig. 1. The calculations were performed for input size $x = 20$ with angular resolution 2° , particle refractive index $n_1 = 1.5$, refractive index of the outer medium $n_2 = 1$, and ratio of scattered to incident wavelengths $\lambda/\lambda_0 = 1.196$. For comparison, this figure also shows the phase function of Mie scattering calculated for the same parameters. In contrast to Mie scattering, which possesses a strong peak in the forward direction, the inelastic V_V component does not vary significantly with angle; it is just twice increased in backward direction. The H_H component has a characteristic minimum at 90° scattering, which is typically observed in fluorescence measurements from dye droplets.^{26,27} Another important difference from Mie scattering is the depolarization of inelastic scatter. The depolarization of the internal field

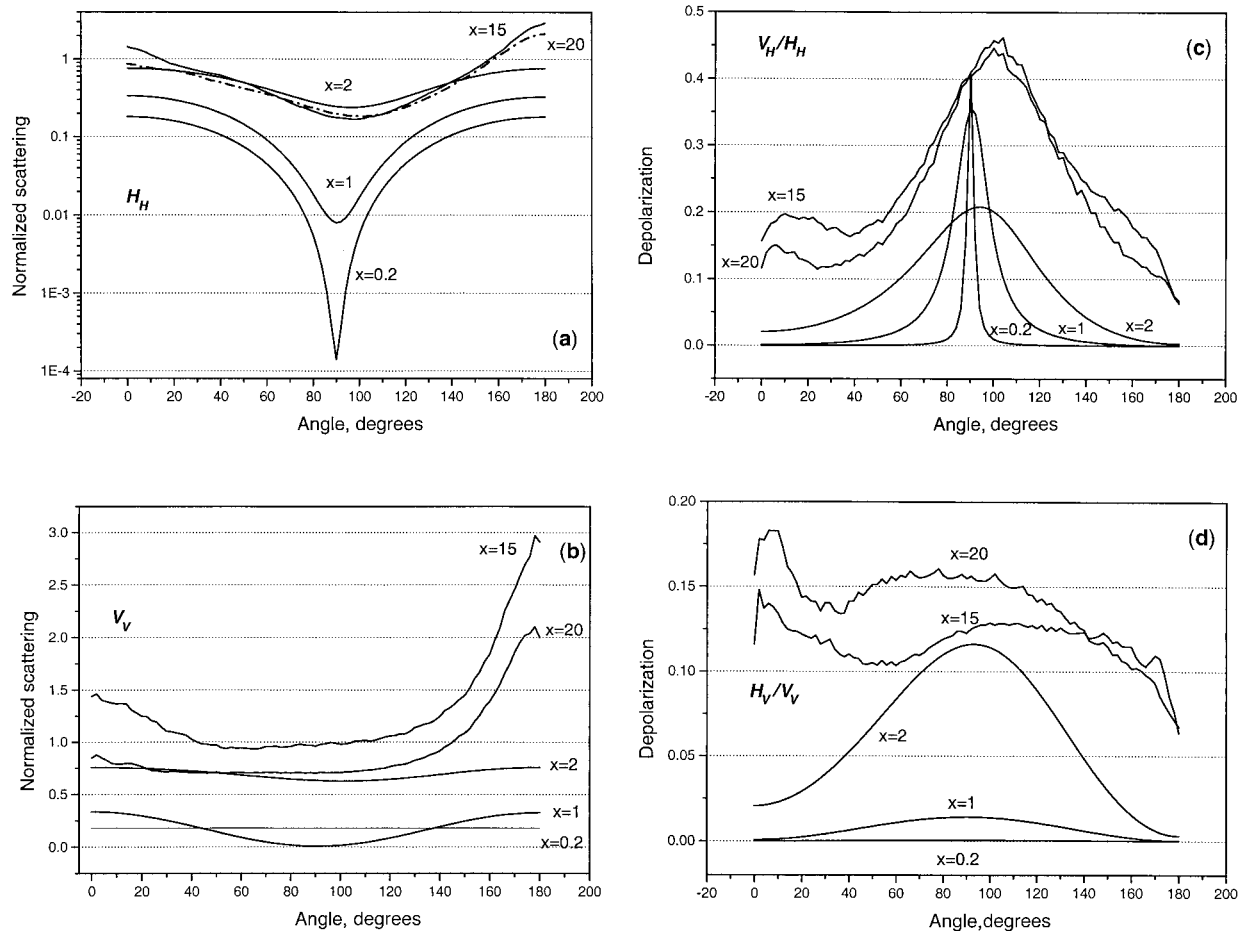


Fig. 2. Components H_H and V_V and their depolarizations V_H/H_H and H_V/V_V as functions of scattering angle for sizes $x = 0.2, 1, 2, 15, 20$. Refractive index, $n_1 = 1.5$; $\lambda/\lambda_0 = 1.196$.

gives rise to nonzero values of depolarized scattered radiances V_H and H_V , which are specific properties of incoherent scattering.

To illustrate the evolution of angular distribution with change in size, in Fig. 2 we show components H_H and V_V together with their depolarization ratios as a function of scattering angle for sizes $x = 0.2, 1, 2, 15, 20$. The values $n_1 = 1.5$ and $\lambda/\lambda_0 = 1.196$ are taken from the paper of Kerker and Druger,²¹ so we can compare the results obtained with the two algorithms. The angular dependence of H_H shown in Fig. 2(a) corresponds to that of Fig. 5 of Ref. 21, and for these sizes our results are in agreement with the calculations of Kerker and Druger.²¹ For $x = 0.2$ a nearly $\cos^2\theta$ dependence of H_H is observed; with increasing size, the deep minimum at 90° is filled in. The scattering of, a wave with vertical polarization for $x < 0.2$ does not depend on the angle [Fig. 2(b)]. For $x = 1$ the scattering is decreased at 90° but rises for the forward and the backward directions; for $x > 15$ the minimum at 90° disappears, and backward scattering exceeds forward scattering by a factor of 2–3.

Figures 2(c) and 2(d) present the angular dependence of depolarization of radiances H_H and V_V . The depolarizations are calculated as ratios V_H/H_H and

H_V/V_V . For H wave the minimum of H_H at 90° results in strong depolarization at this angle: even a small depolarization of the internal field leads to more-efficient scattering of V_H than of H_H . But with the rise of size x , the depolarization peak becomes wider and its amplitude decreases. For $x > 2$ the depolarization of wave H rises at all angles. For small sizes ($x < 0.2$) the depolarization of V wave is absent, but depolarization starts when the size increases. Still, the depolarization of V wave is less than that of H wave, and it does not exceed 20%.

The dependence of intensities V_V and H_H scattered at $\theta = 90^\circ, 180^\circ$ on size is shown in Fig. 3 for refractive indices $n_1 = 1.5, 1.33$. This dependence includes a nonresonant background and narrow resonances. Calculations were performed up to $x = 70$ in steps of $\Delta x = 0.005$. The results are smoothed with a $\Delta x_{\text{sm}} = 0.05$ window to make visible the behavior of the nonresonant background. For a Pentium III PC such a calculation takes ~ 100 h for every value of the refractive index. As was shown in Subsection 2.B of our previous paper,²⁴ for small sizes ($x < 0.01$) the normalized scattered intensity is size independent. In the interval $0.01 < x < 10$ the normalized scattering rises until it reaches a constant level: It becomes proportional to the volume of a

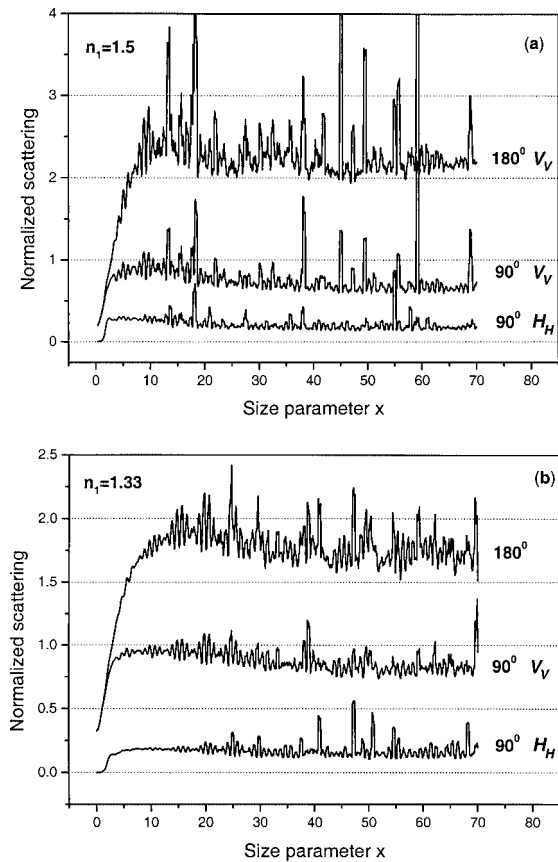


Fig. 3. Normalized components V_V and H_H versus size at scattering angles 180° and 90° . Calculations were performed for $n_1 = 1.5$ and $n = 1.33$ in steps of $\Delta x = 0.005$. The results are smoothed over interval $\Delta x_{sm} = 0.05$.

microsphere. For $n_1 = 1.5, 1.33$ at $\theta = 180^\circ$ the asymptotic nonresonant values are $V_V \sim 2.2, 1.75$, at $\theta = 90^\circ$ these values are $V_V \sim 0.65, 0.8$ and $H_H \sim 0.2, 0.15$. The ratio of power scattered at 180° and 90° (I_{180}/I_{90}) rises as the refractive index increases: For vertical polarization $I_{180}/I_{90} = 3.4, 2.2$ for $n_1 = 1.5, 1.33$, respectively. The calculations of Hill *et al.*³³ for rapidly rotated dipoles ($x \sim 70, n_1 = 1.36$) lead to the value $I_{180}/I_{90} \sim 1.9$. The same ratio for oriented dipoles calculated by Velesco and Schweiger³⁵ in a geometrical optics approximation for big spheres with $n_1 = 1.33$ is $I_{180}/I_{90} = 2.9$. The results of our calculations are in reasonable agreement with the backscattering enhancement observed in fluorescence experiments³⁶; thus, for $n_1 = 1.59$ and $n_1 = 1.34$ the experimentally measured ratios are $I_{180}/I_{90} = 3.2 \pm 0.3$ and $I_{180}/I_{90} = 2.0 \pm 0.3$, respectively.

The depolarization of components V_V and H_H as a function of size for at $\theta = 90^\circ, 180^\circ$ is plotted in Fig. 4. The calculations were performed for refractive index $n_1 = 1.5$, and rest of parameters are the same as for Fig. 3. The depolarization also shows the non-resonant background and narrow peaks that result from MDR. For $x > 20$ the background depolarization of the V_V component at both $\theta = 90^\circ, 180^\circ$ is $\sim 10\%$, which agrees with the low depolarization ob-

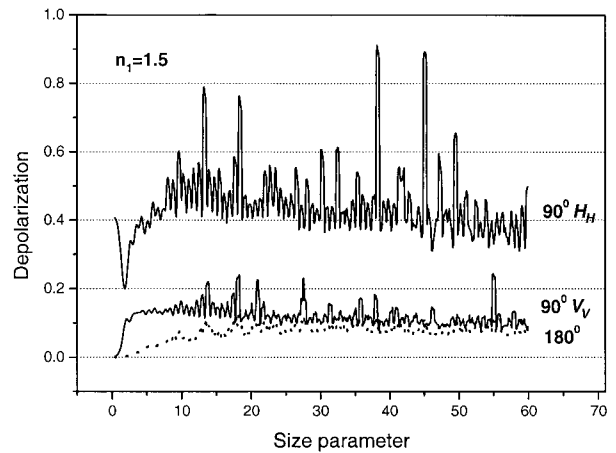


Fig. 4. Depolarization of components V_V and H_H for scattering at 90° and 180° angles. Calculations were performed for $n_1 = 1.5$ and $n = 1.33$ in steps of $\Delta x = .005$. The results are smoothed over interval $\Delta x_{sm} = 0.05$.

served by Fung and Tang.²⁸ The depolarization of H_H at 90° for small radii ($x < 0.5$) is $\sim 40\%$, and it decreases in the $0.5 < x < 2$ range. Such a decrease may be understood from Fig. 2, where the minimum of H_H at 90° scattering is filled in as the microsphere's increases. For $x > 2$, depolarization starts rising; it reaches $\sim 40\%$. Hence at 90° the incident waves

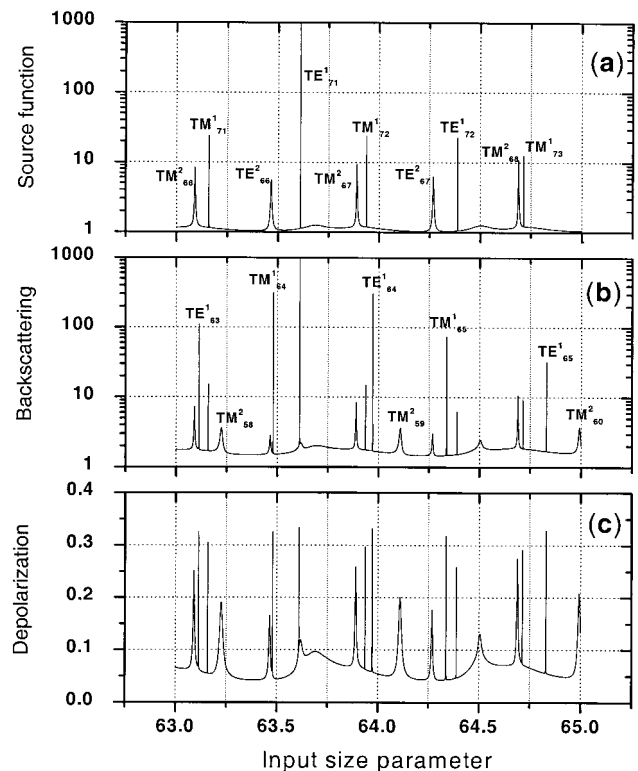


Fig. 5. Normalized volume-averaged source function, inelastic backscattering, and depolarization, all relative to input size parameter. Refractive index, $n_1 = 1.33$; wavelength shift, $\lambda/\lambda_0 = 1.1$; calculation increment, $\Delta x = 0.0001$.

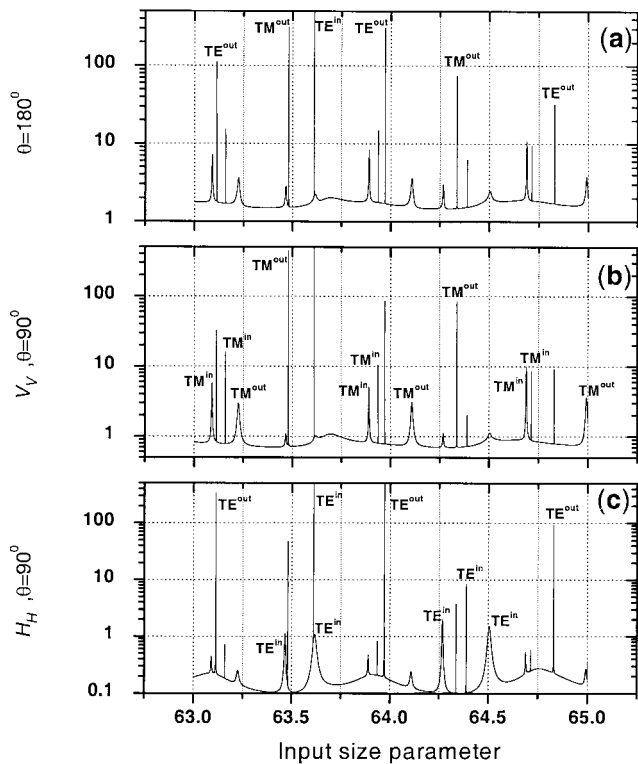


Fig. 6. Normalized inelastic scattering at (a) 180° and 90° observation angles for (b) vertical and (c) horizontal orientation of incident wave polarization. Refractive index, $n_1 = 1.33$; wavelength shift, $\lambda/\lambda_0 = 1.1$; calculation increment, $\Delta x = 0.0001$.

with vertical and horizontal orientation are depolarized differently.

B. Morphology-Dependent Resonances

The effect of MDR on the intensity of scattered light was studied extensively, both theoretically and experimentally.^{1-4,6-12,38-41} The experimental studies were performed mainly at 90° scattering geometry, whereas in the calculations usually only the resonances of integrated over solid-angle Raman power were considered. Hence neither the angular dependence nor the polarization properties of MDR were studied. In this section we present the simulation results, illustrating the influence of MDR on scattered power and depolarization for several scattering angles and orientations of the incident wave polarization.

For separation of input and output MDRs it is convenient to consider the scattered power together with the resonances of the internal field (source function).

A normalized volume-averaged source function is represented by a ratio $\int_v |\mathbf{E}_1|^2 dv/v$, where $v = (4/3)/\pi a^3$ is a particle volume and \mathbf{E}_1 is the internal field.

Figure 5 shows a normalized volume-averaged source function, V_V intensity, and depolarization at $\theta = 180^\circ$ versus input size in the $63.0 < x < 65.0$ range. The refractive index is $n_1 = 1.33$, the wavelength shift is $\lambda/\lambda_0 = 1.1$, and the calculation is performed in steps of $\Delta x = 0.0001$. The input and

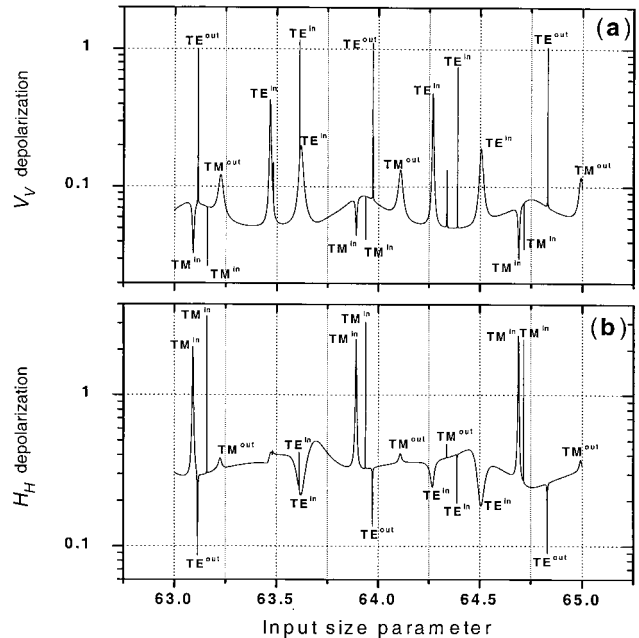


Fig. 7. Depolarization of radiation scattered at 90° for (a) vertical and (b) horizontal orientation of incident wave polarization. Refractive index, $n_1 = 1.33$; wavelength shift, $\lambda/\lambda_0 = 1.1$; calculation increment, $\Delta x = 0.0001$.

output resonances are shown in Figs. 5(a) and 5(b), respectively. The resonances were identified by use of the Guimaraes–Nussenzveig⁴² algorithm. The power scattered in resonance may exceed the background value by as much as 3 orders of magnitude. The output resonances in Fig. 5 in general are higher than the input resonances, except for TE_{71}^1 , which is the double resonance. For the sizes of the corresponding MDRs the scattered radiation is strongly depolarized, probably as a result of multiple traveling of the resonant wave inside the sphere.

The relative intensities of the resonances should be different at 180° and 90° angles. Figure 6 shows the dependence of MDR intensity on size at $\theta = 90^\circ$ for vertically and horizontally oriented incident wave polarization. The calculations were performed for the same parameters as in Fig. 5. The calculation at 90° with $\Delta x = 0.0001$ resolution took approximately two weeks for a Pentium III PC. In Fig. 6(a) we show also the MDR at $\theta = 180^\circ$ for comparison. The positions of MDR at 180° and 90° coincide, but the relative intensities of the TE and TM modes become different. For V wave the TM modes are excited more efficiently, whereas for wave H the TE modes are preferable.

Figure 7 illustrates the influence of MDR on depolarization of 90° scattered radiance. For 90° scattering, this influence becomes more complicated when it is compared with backward scattering, because it depends on the mode type. For V wave the depolarization at TM resonance decreases and the depolarization at TE resonance increases. For H wave the situation is the opposite. Such behavior

can easily be understood. For example, high depolarization of the H_H component at 90° in the absence of resonance is the result of the low scattering efficiency of H wave compared with that of V wave. TE resonances increase the efficiency of H -wave scattering and as a result the depolarization, which we calculate as the ratio V_H/H_H , decreases. For TM resonance, on the contrary, the efficiency of V -wave scattering will rise, and as a result the depolarization ratio will rise also. It should be mentioned that depolarization ratio V_H/H_H may be greater than 1, because of highly efficient scattering of the depolarized component at resonance.

There is also a difference between the influence of input and output resonance on depolarization. For V wave [Fig. 7(a)] the maximal drop of depolarization is observed for TM^{inp} resonance, and the same resonance produces the highest depolarization for H wave [Fig. 7(b)]. The depolarization behavior becomes especially complicated for double resonance; for a example, the TE^1_{71} resonance in Fig. 7(b) appears as a peak inside the dip.

The MDRs also modify the scattering phase function. The angular distribution of scattered radiation at sizes that correspond to various TE and TM resonances is shown in Fig. 8. Figure 8(a) shows the angular distribution of inelastic scatter for $x = 63.02$, which corresponds to the out-of-resonance value. For this size the angular distribution is close to that shown in Fig. 1, and it does not exhibit significant oscillation. The distribution becomes different when the size matches that of a MDR. For the TM mode the V_V component is strongly enhanced at all angles, and the phase function becomes oscillatory [Fig. 8(b)]. For TE resonances [Fig. 8(c)], on the contrary, component H_H is scattered more efficiently, and its angular distribution exhibits strong oscillation. Such oscillations of angular emission were observed, for example, in experiments with stimulated Raman scattering in ethanol droplets⁴³ when one mode was resonant. The modification of the angular distribution of component V_V or H_H for different types of weak MDR was numerically simulated also by Vlesco and Schweiger³⁴ with the use of a geometrical optics approximation. Their results are in a qualitative agreement with ours, although they did not resolve the angular resonant structure.

C. Application to Raman Lidar

A stimulus for performing this research was our desire to apply Raman lidar to the study of cloud water droplets. To obtain quantitative information about liquid water content from lidar measurements it is necessary to know the droplet's Raman backscattering cross section relatively to that of bulk water and its dependence on droplet size. The use of formulas derived for backscattering geometry in our previous paper²⁴ permits the simulation of scattering by big particles. Figure 9 shows normalized Raman backscatter and depolarization as functions of size parameter. Calculations up to $x = 500$ were performed for refractive index $n_1 = 1.33$ in steps of $\Delta x = 0.05$. The

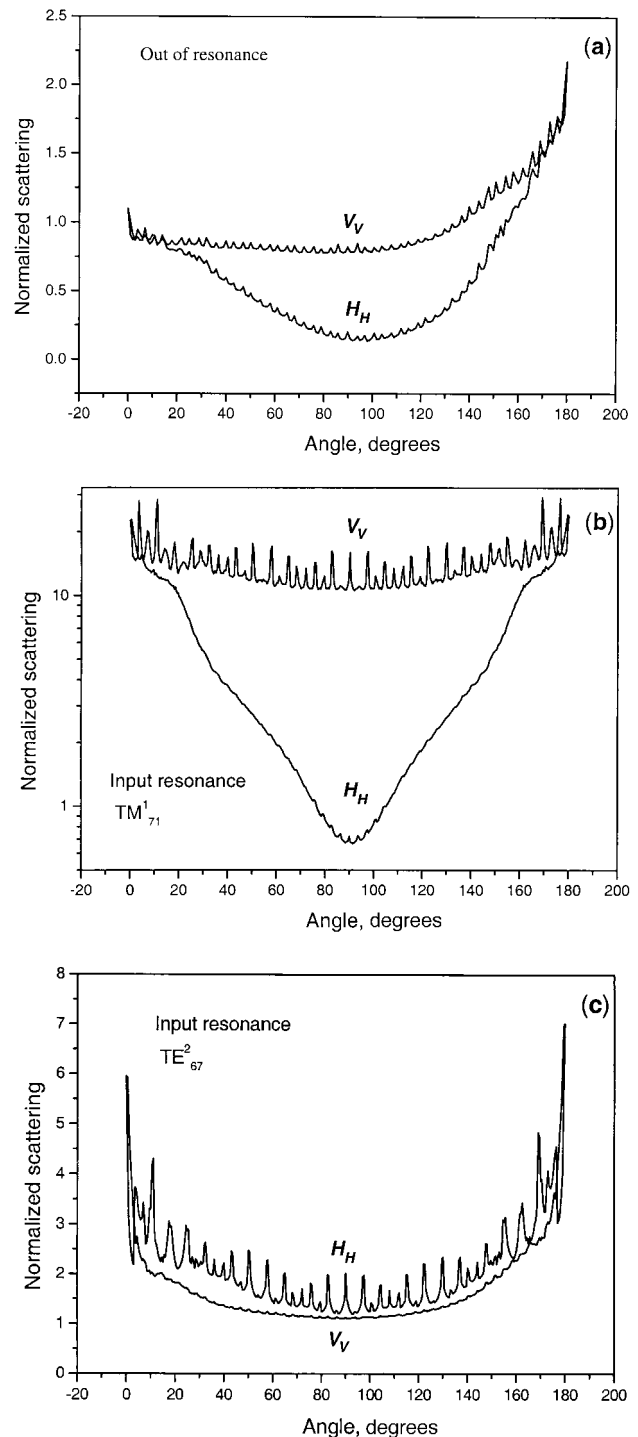


Fig. 8. Angular distribution of components V_V and H_H for the input size parameters that correspond to the (a) out-of-resonance value and to resonances (b) TM^1_{71} and (c) TE^2_{67} . Calculations were performed in angular increments of $\Delta\theta = 0.5^\circ$, and $n_1 = 1.33$.

results for depolarization were smoothed over intervals of $\Delta x_{av} = 0.5$. For $x > 20$ the Raman power is proportional to the droplet volume. Figure 9 does not reveal all resonances, especially for large sizes, because the value of Δx used is insufficient to catch them all. To estimate the contributions of MDR to

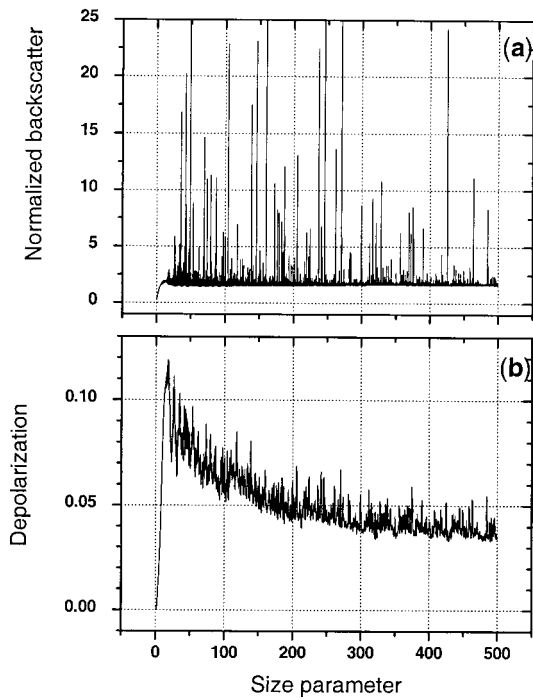


Fig. 9. Dependence of normalized Raman backscatter and depolarization on input size parameter. Calculations were performed in steps of $\Delta x = 0.05$ for refractive index $n_1 = 1.33$, $\theta = 180^\circ$, and $\lambda/\lambda_0 = 1.1$. The results for depolarization are smoothed over interval $\Delta x_{av} = 0.5$.

full Raman backscatter we performed the calculations in $\Delta x = 5 \times 10^{-5}$ steps at $x = 60\text{--}65$, $x = 100\text{--}105$, and $x = 200\text{--}205$ intervals. The integration over resonances gives the average scattered power $V_V \sim 2$ for $x = 60, 100$. For $x = 200$ the scattering is a little less, $V_V \sim 1.9$, which may be the result of an insufficiently small calculation step or an insufficient number of multipole coefficients l_{max} used for such large-sized microspheres. We calculated $l_{max} = x + 4x^{1/3} + 2$, which is good enough for elastic scattering with plane-wave incidence but is probably not sufficient for high- Q resonances in the internal fields that generate Raman scattering. From the simulation that we performed we can conclude that the normalized Raman backscattering cross section does not depend significantly on droplet size and that the backscattering from droplets exceeds the corresponding value for bulk water by approximately a factor of 2.

The depolarization of Raman backscatter as a function of size is plotted in Fig. 9(b). The maximal depolarization of 12% is achieved at $x \sim 10$; for a larger size it decreases to 4%. The depolarization of bulk water inside the part of Raman contour that can be used for lidar sounding is approximately 15–20%.⁴³ Hence the additional depolarization introduced by the droplets probably cannot be reliably detected in lidar measurements. The experimentally observed enhanced depolarization of Raman backscatter in the lidar measurements of liquid water³² should be attributed to other effects, such as solid inclusions in

water aerosol and the influence of rotational Raman spectra of water vapor.

The results presented here were obtained for a rather idealized situation. The real Raman contour of liquid water extends from ~ 3100 to $\sim 3600 \text{ cm}^{-1}$ (Ref. 25). The bandwidth of receiving filters in lidars is typically $\sim 3 \text{ nm}$, so the ratio of Raman to incident wavelength for a 355-nm pump varies from 1.12 to 1.13, which will smooth the MDR signatures. Even stronger smoothing of MDR will be produced by the size distribution of droplets in real cloud, for which the radii may vary in the 0.5–20- μm range. Still this smoothing does not affect the main result: The Raman scatter is proportional the droplet volume, so the simultaneous measurement of Raman and elastic lidar signals permits the retrieval of droplet size.³¹

3. Conclusions

The program that we have developed permits the calculation of angular and polarization characteristics of Raman scattering for a wide range of microdroplet sizes. Although it is simplified, the dipole model describes the basic properties of incoherent Raman scattering and is in agreement with existing experimental results. For an incident wave with vertical polarization, the phase function does not vary strongly with angle, and only in the backward direction is there an enhancement to compare with bulk medium scattering. For $n_1 = 1.33$ this enhancement is of a factor of 2.

The effect of MDR modifies the angular distribution of Raman intensity. For size parameters that correspond to TM or TE resonance, the enhancement of the V_V or the H_H component, respectively, is observed. The angular distribution of the enhanced component becomes oscillatory. MDR also influences the depolarization of Raman scattering. For backward scattering, all types of MDR increase the depolarization. The depolarization at 90° may be either enhanced or diminished, depending on the resonance type (TE or TM) and on the orientation of the incident radiation polarization.

The algorithm developed here requires additional improvement to match experimental results. In our model we suggested that the Raman bands have zero depolarization, but, in reality, depolarization always occurs. Accounting for molecular anisotropy will not strongly influence the results for V wave, but for H wave the polarization characteristics of scattered radiation as well as the scattering cross section may be different. For accurate description of Raman scattering in this case, the induced dipoles should be calculated through a “derived polarizability tensor” as was suggested in Ref. 23, and doing this is one of our goals for the near future. The calculation speed may be further increased by use of a variable step: fine in the vicinity of MDR and coarse between the resonances.³⁷ But even at this stage our program improves our understanding of the main features of incoherent Raman scattering and aids in the realization of one of our main goals: quantifying the char-

acteristics of Raman scattering by water droplets for validation of Raman lidar measurements of clouds.

References

1. H.-M. Tzeng, K. F. Wall, M. B. Long, and R. K. Chang, "Evaporation and condensation rates of liquid droplets deduced from structure resonances in the fluorescence spectra," *Opt. Lett.* **9**, 273–275 (1984).
2. R. Thurn and W. Kiefer, "Structural resonances observed in the Raman spectra of optically levitated liquid droplets," *Appl. Opt.* **24**, 1515–1519 (1985).
3. G. Schweiger, "Raman scattering on single aerosol particles and on flowing aerosols: a review," *J. Aerosol. Sci.* **21**, 483–509 (1990).
4. G. Schweiger, "Raman scattering on microparticles: size dependence," *J. Opt. Soc. Am. B* **8**, 1770–1778 (1991).
5. K. H. Fung and I. N. Tang, "Relative Raman scattering cross-section measurements with suspended particles," *Appl. Spectrosc.* **45**, 734–737 (1991).
6. J. Popp, M. Lankers, K. Schaschek, W. Kifer, and J. T. Hodges, "Observation of sudden temperature jumps in optically levitated microdroplets due to morphology-dependent input resonances," *Appl. Opt.* **34**, 2380–2386 (1995).
7. T. Kaiser, G. Roll, and G. Schweiger, "Investigation of coated droplets in an optical trap: Raman-scattering, elastic-light-scattering and evaporation characteristics," *Appl. Opt.* **35**, 5918–5924 (1996).
8. R. Vehring, "Linear Raman spectroscopy on aqueous aerosols: influence of nonlinear effects on detection limits," *J. Aerosol. Sci.* **29**, 65–79 (1998).
9. R. Vehring, C. L. Aardahl, G. Schweiger, and E. J. Davis, "The characterization of fine particles originating from an uncharged aerosol: size dependence and detection limits for Raman analysis," *J. Aerosol. Sci.* **29**, 1045–1061 (1998).
10. J. Popp, M. Lankers, M. Trunk, I. Hartmann, E. Urlaub, and W. Kiefer, "High-precision determination of size, refractive index, and dispersion of single microparticles from morphology-dependent resonances in optical processes," *Appl. Spectrosc.* **52**, 284–291 (1998).
11. J. Musick, J. Popp, M. Trunck, and W. Kiefer, "Investigations of radical polymerization and copolymerization reactions in optically levitated microdroplets by simultaneous Raman spectroscopy, Mie scattering, and radiation pressure measurements," *Appl. Spectrosc.* **52**, 692–701 (1998).
12. R. Pastel and A. Struthers, "Measuring evaporation rates of laser-trapped droplets by use of fluorescent morphology-dependent resonances," *Appl. Opt.* **40**, 2510–2514 (2001).
13. M. A. Stowers and S. K. Friedlander, "Chemical characterization of flowing polydisperse aerosols by Raman spectroscopy," *Aerosol Sci. Technol.* **36**, 48–61 (2002).
14. S. C. Hill, H. I. Saleheen, M. D. Barnes, and W. B. Whitten, "Modeling fluorescence collection from single molecules in microspheres: effects of position, orientation, and frequency," *Appl. Opt.* **35**, 6278–6288 (1996).
15. P. H. Kaye, J. E. Barton, E. Hirst, and J. M. Clark, "Simultaneous light scattering and intrinsic fluorescence measurement for the classification of airborne particles," *Appl. Opt.* **39**, 3738–3745 (2000).
16. S. C. Hill, R. G. Pinnick, S. Niles, N. F. Fell, Y. L. Pan, J. Bottiger, B. V. Bronk, S. Holler, and R. K. Chang, "Fluorescence from airborne microparticles: dependence on size, concentration of fluorophores, and illumination intensity," *Appl. Opt.* **40**, 3005–3013 (2001).
17. H. Chew, P. J. McNulty, and M. Kerker, "Model for Raman and fluorescent scattering by molecules embedded in small particles," *Phys. Rev. A* **13**, 396–404 (1976).
18. H. Chew, M. Kerker, and P. J. McNulty, "Raman and fluorescent scattering by molecules embedded in concentric spheres," *J. Opt. Soc. Am.* **66**, 440–444 (1976).
19. H. Chew, "Total fluorescent scattering cross section," *Phys. Rev. A* **37**, 4107–4110 (1988).
20. M. Kerker, P. J. McNulty, M. Sculley, H. Chew, and D. D. Cooke, "Raman and fluorescent scattering by molecules embedded in small particles: results for incoherent optical processes," *J. Opt. Soc. Am.* **68**, 1676–1686 (1979).
21. M. Kerker and S. D. Druger, "Raman and fluorescent scattering by molecules embedded in spheres with radii up to several multiples of the wavelength," *Appl. Opt.* **18**, 1172–1179 (1979).
22. S. D. Druger and P. J. McNulty, "Radiation patterns of fluorescence from molecules embedded in small particles: general case," *Appl. Opt.* **22**, 75–82 (1983).
23. S. D. Druger and P. J. McNulty, "Radiation pattern of Raman scattering from randomly oriented molecules in or near small particles," *Phys. Rev. A* **29**, 1545–1547 (1984).
24. V. Griaznov, I. Veselovskii, A. Kolgotin, and D. N. Whiteman, "Angle- and size-dependent characteristics of incoherent Raman and fluorescent scattering by microspheres. 1. General expressions," *Appl. Opt.* (to be published).
25. J. R. Scherer, M. K. Go, and S. Kint, "Raman spectra and structure of water from -10 to 90° ," *J. Phys. Chem.* **78**, 1304–1313 (1974).
26. J. P. Kratochvil, M.-P. Lee, and M. Kerker, "Angular distribution of fluorescence from small particles," *Appl. Opt.* **17**, 1978–1980 (1978).
27. E.-H. Lee, R. E. Benner, J. B. Fenn, and R. K. Chang, "Angular distribution of fluorescence from monodispersed particles," *Appl. Opt.* **17**, 1980–1982 (1978).
28. K. H. Fung and I. N. Tang, "Polarization measurements on Raman scattering from spherical droplets," *Appl. Spectrosc.* **46**, 1189–1192 (1992).
29. D. N. Whiteman, S. H. Melfi, and R. A. Ferrare, "Raman lidar system for measurement of water vapor and aerosols in the Earth's atmosphere," *Appl. Opt.* **31**, 3068–3082 (1992).
30. S. H. Melfi, K. D. Evans, J. Li, D. Whiteman, R. Ferrare, and G. Schwemmer, "Observation of Raman scattering by cloud droplets in the atmosphere," *Appl. Opt.* **36**, 3551–3559 (1997).
31. D. N. Whiteman and S. H. Melfi, "Cloud liquid water, mean droplet radius, and number density measurements using a Raman lidar," *J. Geophys. Res.* **104**, 31,411–31,419 (1999).
32. I. A. Veselovskii, H. K. Cha, D. H. Kim, S. C. Choi, and J. M. Lee, "Raman lidar for the study of liquid water and water vapor in troposphere," *Appl. Phys. B* **71**, 113–117 (2000).
33. I. A. Veselovskii, H. K. Cha, D. H. Kim, S. C. Choi, and J. M. Lee, "Study of atmospheric water in gaseous and liquid state by using combined elastic-Raman depolarization lidar," *Appl. Phys. B* **73**, 739–744 (2001).
34. S. C. Hill, Y.-L. Pan, S. Holler, and R. K. Chang, "Enhanced backward-directed multiphoton-excited fluorescence from dielectric microcavities," *Phys. Rev. Lett.* **85**, 54–57 (2000).
35. N. Velesco and G. Schweiger, "Geometrical optics calculation of inelastic scattering on large particles," *Appl. Opt.* **38**, 1046–1052 (1999).
36. Y. L. Pan, S. C. Hill, J. P. Wolf, S. Holler, R. K. Chang, and J. R. Bottiger, "Backward-enhanced fluorescence from clusters of microspheres and particles of tryptophan," *Appl. Opt.* **41**, 2994–2999 (2002).
37. S. C. Hill, R. E. Benner, C. K. Rushfort, and P. R. Conwell, "Structural resonances observed in the fluorescence emission from small spheres on substrates," *Appl. Opt.* **23**, 1680–1683 (1984).
38. S. C. Hill, C. K. Rushforth, R. E. Benner, and P. R. Conwell, "Sizing dielectric spheres and cylinders by aligning measured and computed resonance locations — algorithm for multiple orders," *Appl. Opt.* **24**, 2380–2390 (1985).

39. A. Biswas, H. Latifi, R. L. Armstrong, and R. G. Pinnick, "Double-resonance stimulated Raman scattering from optically levitated glycerol droplets," *Phys. Rev. A* **40**, 7413–7416 (1989).
40. J. D. Eversole, H. B. Lin, and A. J. Campillo, "Input–output resonance correlation in laser induced emission from microdroplets," *J. Opt. Soc. Am. B* **12**, 287–296 (1995).
41. H. B. Lin and A. J. Campillo, "cw nonlinear optics in droplet microcavities displaying enhanced gain," *Phys. Rev. Lett.* **73**, 2440–2443 (1994).
42. L. G. Guimaraes and H. M. Nussenzveig, "Uniform approximation of Mie resonances," *J. Mod. Opt.* **41**, 625–647 (1994).
43. G. Chen, W. P. Acker, R. K. Chang, and S. C. Hill, "Fine structures in the angular distribution of stimulated Raman scattering from single droplets," *Opt. Lett.* **16**, 117–119 (1991).
44. K. Cunningham and P. A. Lyons, "Depolarization ratio studies on liquid water," *J. Chem. Phys.* **59**, 2132–2139 (1973).